Available online at www.sciencedirect.com
SCIENCE DIRECT®
Journal of Magnetic Resonance 178 (2006) 56–64
JMR Journal of Magnetic Resonance
www.elsevier.com/locate/jmr

Novel ^{13}C direct detection experiments, including extension to the third dimension, to perform the complete assignment of proteins

Wolfgang Bermel [a], Ivano Bertini [b,*], Isabella C. Felli [b], Rainer Kümmerle [c], Roberta Pierattelli [b]

[a] *Bruker BioSpin GmbH, Rheinstetten, Germany*
[b] *Magnetic Resonance Center and Department of Chemistry, University of Florence, Italy*
[c] *Bruker BioSpin AG, Fällanden, Switzerland*

Received 28 June 2005; revised 22 August 2005
Available online 30 September 2005

Abstract

Carbon-13 direct detection NMR methods are feasible thanks to the improvements in probehead technology and to the development of new NMR experiments. We present here a complete set of experiments, based on C′ direct detection, developed to perform protein complete assignment of backbone and side-chains (except for aromatic rings). This strategy offers alternative solutions for demanding situations (paramagnetic and/or large molecules) and can be useful in general in conjunction with conventional experiments.

Keywords: Protonless NMR; ^{13}C NMR; ^{13}C-direct detection; Sequential assignment; Protein structure

1. Introduction

Although reports on ^{13}C NMR spin-system assignment of ^{13}C enriched proteins are available in the literature since 1988 [1–3], heteronuclear detected NMR experiments have been progressively abandoned in favor of ^{1}H-detected experiments. Indeed, the higher efficiency of proton NMR prompted the design of a vast number of inverse-detected experiments for biomolecular applications. After the advent of TROSY spectroscopy, which is able to reduce the adverse effect of transverse relaxation on the NH fragments of peptide bonds, or in aromatic CH groups [4], the assignment of the backbone nuclei in triply labeled (^{15}N, ^{13}C, ^{2}H) monomeric proteins as large as 80 kDa became feasible [5]. More recently also methyl and methylene TROSY experiments have been proposed [6,7]. The cross relaxation-enhanced polarization transfer (CRINEPT) technique optimized for large systems provided another increase in the molecular size limit for NMR studies [8,9]. These techniques are mainly used for backbone assignment and seldom the assignment of side-chains in large molecules is attempted.

Experiments that rely on heteronuclei, in particular on ^{13}C, were recently applied to several paramagnetic proteins, where the contribution to line broadening from the paramagnetic center is so large that ^{1}H signals are broadened beyond detectable limits in a wide sphere around the metal ion [10–14]. These applications promoted the *revival* of heteronuclear NMR as a means to overcome the limitations imposed to ^{1}H NMR by fast proton transverse relaxation [15–17]. The interest in ^{13}C NMR has also triggered a renewal of interest in probe design to overcome the limit of sensitivity of low-γ nuclei, and the consequent increase in spectrometer performance prompted the design of novel applications, opening new possibilities of exploitation of heteronuclear NMR [18,19].

A ^{13}C-based approach to obtain the heteronuclear backbone assignment was first proposed [20,21] and extended to

* Corresponding author. Fax: +39 055 4574271.
E-mail address: ivanobertini@cerm.unifi.it (I. Bertini).

1090-7807/$ - see front matter © 2005 Elsevier Inc. All rights reserved.
doi:10.1016/j.jmr.2005.08.011

the side-chains with a CBCACO experiment [22], that yields correlations between three nuclei (C^{β}, C^{α} and C') and to the rest of the chain with TOCSY-type experiments [15,22,23]. The problem of signal splitting due to ^{13}C–^{13}C scalar couplings in the direct-dimension was solved for C' and for C^{α} nuclei through the IPAP and DIPAP approaches, respectively [22,24].

We would like to present here a set of novel experiments to supplement the already proposed 2D CACO-IPAP [22], 3D CBCACO-IPAP [22], and 3D CANCO [20,21] experiments, that enable the complete NMR assignment of a protein based on direct detection of C' (except for aromatic rings). The new features of these experiments include extension to the complete side chains (CCCO-IPAP), 3D experiments with ^{15}N evolution in one of the indirect dimensions (3D CBCACON and 3D CCCON) and inclusion of a spin state selective approach (IPAP or S^3E) in all experiments to improve resolution in the direct acquisition dimension (including CON and CANCO). These experiments are demonstrated on a monomeric analogue of reduced human Cu,Zn superoxide dismutase, and we will show that with a limited number of experiments it is possible to obtain the complete assignment of a protein *without involving ^1H-transfer or TROSY effects*. The limits of the approach, particularly with respect to the experimental time needed to accomplish the assignment, will also be discussed.

2. Results and discussion

The sample used in this research is human Cu,Zn superoxide dismutase modified at point 50, 51 (Phe, Gly → Glu), and 133 (Glu → Gln). The first two mutations disrupt the quaternary structure of the protein producing a soluble monomeric form [25] (MW 16,000) while the third mutation increases the enzymatic activity [26]. This monomeric analog (SOD hereafter) has been expressed to large quantity and widely characterized. The NMR solution structure of the Cu(I) form has been solved [27] and a fairly extended assignment of this protein is available from literature data [28]. It thus constitutes a reliable benchmark for an assignment protocol.

2.1. Experiments for sequence-specific signal assignment

The simplest NMR experiment to verify the quality of a sample is the ^1H–^{15}N HSQC. Indeed, from the dispersion of the signals, it is immediately evident whether the investigated system is suitable for an NMR characterization. The equivalent experiment in a ^{13}C-based strategy is the CON experiment; we report here the IPAP version of the experiment to improve the resolution in the direct acquisition dimension by removing the 55 Hz $J_{C'C}\alpha$-splitting [22].

In Fig. 1 the CON-IPAP spectrum recorded on reduced SOD is reported. The map shows the expected cross peaks with an excellent resolution, including those of Pro residues as well as those of Asn and Gln side-chains. The first count of the cross peaks in the spectrum shows 161 cross peaks

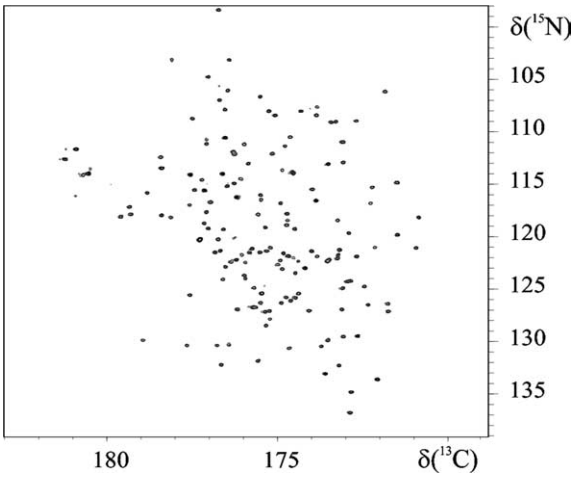

Fig. 1. The 2D CON-IPAP spectrum acquired on SOD with a 14.1 T spectrometer equipped with a cryoprobe optimized for ^{13}C detection at 298 K. The pulse sequence used is reported in Appendix A along with pulse lengths and delay durations; the remaining experimental parameters are reported under Section 3. Treatment of the data prior to Fourier transform was performed as described under Section 3. The data were then multiplied by a cosine window function, zero filled and processed through Fourier transformation, to a matrix of 1024 × 1024.

out of the expected 163 (152 for the backbone and 11 for the Asn and Gln side chains). The same count performed on the ^1H–^{15}N HSQC spectrum shows 159 cross peaks out of the 169 expected ones (147 for the backbone and 22 for Asn and Gln side chains). Two additional peaks in the CON-IPAP map could be identified with a thorough analysis of the spectrum as partially overlapped with two other resonances. On the other hand, the missing NH signals were not revealed in the ^1H–^{15}N HSQC, despite the good quality of the spectra obtainable on the present sample. The missing signals are indeed due to highly mobile and solvent accessible residues [28]. The gain in resolution observed in the CON experiment compared with that of the HSQC is due to the larger dispersion/linewidth of the CO resonances with respect to the HN resonances at the magnetic field used for these experiments (14.1 T). At higher fields, on ^2H labeled proteins with the TROSY approach, the situation will be inverted due to the increase of transverse carbonyl relaxation rates.

The CON-IPAP experiment, together with the CACO-IPAP [22] experiment allows one to identify all backbone correlations. To link the backbone nuclei in a sequence specific manner, the CANCO experiment [20] offers one possible solution. In the present case, thanks to the implementation of the IPAP scheme (see Appendix A), already the 2D map provided good resolution. The intra-residue correlations of 10 residues (20, 49, 55, 57, 60, 110, 137, 144, 146, and 147) are missing. The corresponding inter-residue correlations are all present but one (49–48). Four other inter-residue correlations (50–49, 57–56, 58–57, and 144–143) are partially in overlap with other resonances, and may not be trivial to assign. Additional 32 correlations (16 inter- and 16 intra-residue) are partially overlapped. In

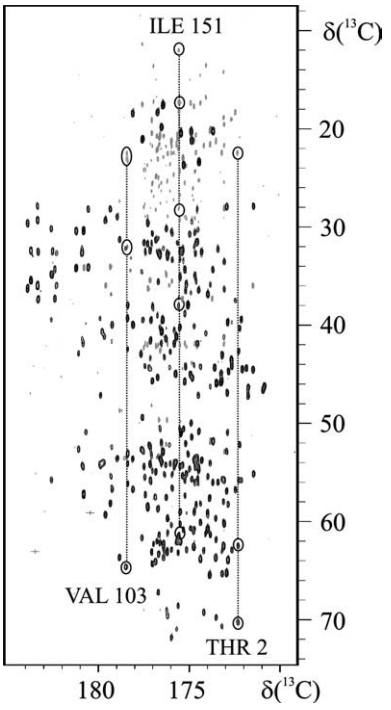

Fig. 2. The 2D CBCACO-IPAP (black contours) is compared with the 2D CCCO-IPAP spectra obtained with different spin-lock times (dark and light grey for the 10 ms and 22 ms spin lock experiments, respectively). Spectra were acquired on monomeric SOD with a 14.1 T spectrometer equipped with a cryoprobe optimized for ^{13}C detection. The spin systems of Thr 2, Val 103, and Ile 151 have been highlighted. The pulse sequence used is reported in Appendix A along with pulse lengths and delay durations; the remaining experimental parameters are reported under Section 3. Treatment of the data prior to Fourier transform was performed as described under Section 3. The data were then multiplied by a cosine window function, zero filled and processed through Fourier transformation, to a matrix of 2048×1024.

general, however, the redundant information available in the spectrum enables the assignment, reducing the number of the unassignable resonances. In the 3D version of the experiment the cases of ^{13}C-chemical shift degeneracy were largely solved due to the ^{15}N dispersion.

To get information on the side chains, we propose the CCCO-IPAP experiment (see Appendix A for the pulse sequence details), that in conjunction with the CBCACO-IPAP experiment [22] provides information on all the carbon atoms in the side chain.[1] The intensity of the cross peaks of each side chain in this experiment is modulated by the length of the spin-lock time, as expected. As an example of the quality of the data, in Fig. 2 the spin-systems corresponding to Thr 2, Val 103 and Ile 151 are highlighted in the overlay of two 2D CCCO-IPAP maps recorded with different spin-lock times and the CBCACO-IPAP map. Overall, 96% of the expected peaks have been identified and assigned. The missing correlations belong to the terminal part of Leu and Ile side-chains.

[1] Except for aromatic rings; in this case additional experiments are necessary to correlate the C^{β} to the aromatic ring.

This is an important step in the assignment procedure, as information on the residue-type becomes available, providing a handle in solving possible ambiguities still present in the backbone assignment, also thanks to the large chemical shift dispersion of carbon atoms in the side chains [29]. Moreover the C^{β} chemical shift values, together with the C^{α} values, also give information useful to determine the secondary-structure propensity of the polypeptidic chain [30,31] to fully exploit the ^{13}C-Chemical Shift Index for a first structural characterization of the protein [31]. This is possible also for the regions where NH was not assigned with the proton-based experiments due to exchange or where prolines are present.

The CCCO-IPAP can easily be expanded to a third dimension by including C^{α} evolution (see Appendix A), as already suggested for the CBCACO-IPAP experiment [22]. This allows one to separate different spin systems that have degenerate C′ chemical shifts, offering an increase in resolution.

If resolution is still a limiting factor, as often the case when dealing with large biomolecules, it is convenient to exploit the backbone ^{15}N-signal dispersion to expand the ^{13}C–^{13}C 2D experiments in a third dimension. The 3D CANCO experiment [20] is conceived as such, as well as the two variants of the selective CANCO designed to discriminate between the sequential and intra-residue correlations [21]. For the ^{13}C-based sequences for side-chain assignment, the insertion of the CON building block in the most sensitive 2D experiments is a suitable solution. To compare the relative sensitivity of these experiments, the first increments are reported in Fig. 3 (top).

By combining the CBCACO-IPAP and the CCCO-IPAP, with the CON-IPAP a set of 3D experiments with C′ in the acquisition dimension, N and $C^{\alpha/ali}$ in the indirect dimension can be obtained. We have implemented the CBCACON-IPAP and the CCCON-IPAP. The three dimensional spectra of these two *exclusively heteronuclear* experiments are shown in Fig. 4 while the pulse sequences are described in detail in Appendix A. The first increments are also reported in Fig. 3 (bottom). The CBCACON-IPAP experiment correlates the C^{α}, C^{β} of each amino acid to the C′ and then to the N of the following amino acid, and the CCCON-IPAP also includes the correlations with the remaining carbons of the side chain, in a similar fashion to the CBCACONH and CCCONH experiments [32].

2.2. The assignment protocol

The set of 3D CANCO-IPAP and of the 3D experiments based on C′ direct detection for side chain assignment (CBCACO-IPAP, CCCO-IPAP, CBCACON-IPAP, and CCCON-IPAP) can be used to identify all the spin systems in the protein involving carbon and nitrogen and to correlate them in a sequence specific manner. To illustrate the sequence specific assignment strategy, Fig. 5 reports the example of Pro 74–Lys 75. It can be observed that the spin system of each amino acid can be easily identified with the

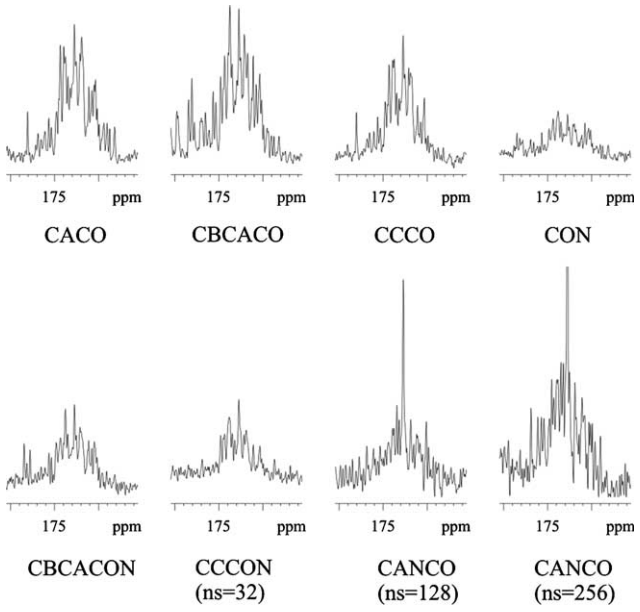

Fig. 3. The first increment of the experiments based on C′ direct detection with the IPAP approach (CACO, CBCACO, CCCO, CON, CBCACON, CCCON, and CANCO) is shown to compare the relative sensitivity. Experiments were acquired at 14.1 T spectrometer equipped with a cryoprobe optimized for ^{13}C detection. All experiments were acquired with comparable parameters and with 16 scans, unless otherwise indicated. The trace is extracted after linear combination of the in-phase and anti-phase components. The pulse sequences used are reported in Appendix A along with pulse lengths and delay durations; the remaining experimental parameters are reported under Section 3. Treatment of the data prior to Fourier transform was performed as described under Section 3. The data were then multiplied by a cosine window function, zero filled to 1024 points and processed through Fourier transformation.

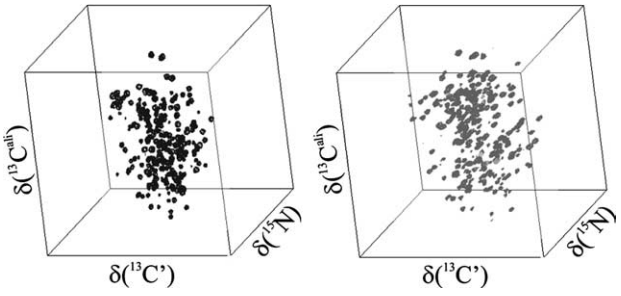

Fig. 4. The 3D CBCACON-IPAP (left) and CCCON-IPAP (right) spectra acquired on SOD with a 14.1 T spectrometer equipped with a cryoprobe optimized for ^{13}C detection. The pulse sequences used are reported in Appendix A along with pulse lengths and delay durations; the remaining experimental parameters are reported in Section 3. Treatment of the data prior to Fourier transform was performed as described under Section 3. The data were then multiplied by a cosine window function, zero filled to $1024 \times 128 \times 256$ points and processed through Fourier transformation.

3D CBCACO, 3D CCCO, 3D CBCACON, and 3D CCCON experiments by correlating the carbon atoms of the side chains to C^{α}_i, C'_i and also to N_{i+1}. Each spin-system can then be linked in a sequence specific manner through the 3D CANCO-IPAP by correlating the C'_i and N_{i+1} to two C^{α} spins (C^{α}_i and C^{α}_{i+1}). In summary the CBCACO, CCCO, CBACON, and CCCON experiments enable identification of the ^{13}C-spin system of each amino acid (that also gives information on the amino acid-type) exploiting the nice chemical shift dispersion of carbonyls and amide nitrogens. The CANCO experiment then provides the sequential link by correlating the C^{α} of two subsequent residues with the carbonyl of the first one and with the amide nitrogen of the second one.

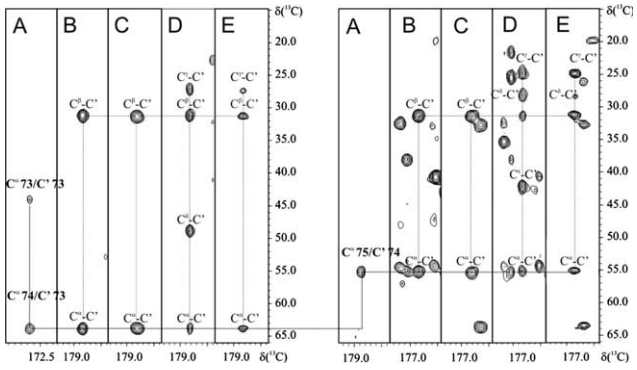

Fig. 5. The assignment strategy based only on ^{13}C direct detection 3D experiments is shown for the fragment Pro 74 (left)–Lys 75 (right) as an example. The portions of $C^{\alpha/ali}$–C′ planes of 3D spectra reported in the figure are taken from the following experiments: (A) 3D CANCO-IPAP, (B) 3D CBCACO-IPAP, (C) 3D CBCACON-IPAP, (D) 3D CCCO-IPAP, and (E) 3D CCCON-IPAP. For each residue, the figure shows in (A) the region of the C^{α}–C′ plane of 3D CANCO at the N_i chemical shift (129.2 ppm for Pro 74, 115.8 ppm for Lys 75), in (B) and (D) a portion of the C^{ali}–C′ plane of the CBCACO and CCCO at the C^{α}_i chemical shift (63.7 ppm for Pro 74, 54.9 ppm for Lys 75), and in (C) and (E) the portions of the C^{ali}–C′ plane of the CBCACON and CCCON at the N_{i+1} chemical shift (115.8 ppm for Lys 75, 121.5 ppm for Asp 76). All experiments were acquired using the IPAP approach that allows us remove the large C^{α}–C′ scalar coupling in the direct dimension.

In Table 1, a list of the ^{13}C-detected experiments proposed for protein signal assignment based on C′ direct detection and tested on SOD is reported. We also report the number of scans suggested for each experiment, estimated on the basis of the signal-to-noise ratio of the first increments reported in Fig. 3 (see Section 3). Summarizing, for a protein of average size like the present one, highly soluble, that can be expressed and isotopically enriched with high yield, the experimental time needed to have the set of 2D spectra is not unreasonably long with respect to the ^{1}H-based experimental approach. Indeed, for monomeric SOD, the whole series of 2D experiments could be acquired in about 2 days, the 3D versions of experiments necessary for spin system identification in 4 days (plus 6 days for the experiments with ^{15}N evolution) and the 3D CANCO in 6 days. Actually the larger dispersion of ^{13}C with respect to ^{1}H allowed us to obtain with this set of experiments a virtually complete assignment. Exchange processes identified for residues 56 and 61 [33] prevent detection of NH correlations for residues 57–59 [28], interrupting the sequential ''walk on the backbone'' with the conventional triple resonance assignment strategy based on NH acquisition [34], did not prevent sequential assignment through the protocol proposed. The same holds for proline residues. The large number of Gly present in

Table 1
The experiments, based on acquisition of C′ with the IPAP approach, that we propose for complete sequence specific assignment of heteronuclei are listed

Experiment	Correlations observed	Scans	Ref.
2D			
CACO-IPAP	C_i^{α}–C_i'	N	[22]
CBCACO-IPAP	C_i^{β}–C_i', C_i^{α}–C_i'	N	[22]
CCCO-IPAP	$C_i^{\beta,\gamma,\delta,\varepsilon}$–$C_i'$, C_i^{α}–C_i'	$2N$	This work
CON-IPAP	N_i–C'_{i-1}	$2N$	[13,14] and this work
CANCO-IPAP	C_i^{α}–C'_{i-1}	$16N$	
	C_{i-1}^{α}–C'_{i-1}		[20] and this work
3D			
CBCACO-IPAP	C_i^{β}–C_i^{α}–C_i', C_i^{α}–C_i^{α}–C_i'	N	[22]
CCCO-IPAP	$C_i^{\beta,\gamma,\delta,\varepsilon}$–$C_i^{\alpha}$–$C_i'$, C_i^{α}–C_i^{α}–C_i'	$2N$	This work
CANCO-IPAP	C_i^{α}–N_i–C'_{i-1}		
	C_{i-1}^{α}–N_i–C'_{i-1}	$16N$	[20] and this work
CBCACON-IPAP	C_{i-1}^{α}–N_i–C'_{i-1}		
	C_{i-1}^{β}–N_i–C'_{i-1}	$2N$	This work
CCCON-IPAP	C_{i-1}^{α}–N_i–C'_{i-1}		
	$C_{i-1}^{\beta,\gamma,\delta,\varepsilon}$–$N_i$–$C'_{i-1}$	$4N$	This work

The correlations that can be observed in each experiment are indicated schematically as well as the number of scans necessary for each experiment, relative to the number of scans necessary to acquire the most sensitive ones (N). These estimates are based on our experience with monomeric reduced SOD.

SOD (24) enables also to exploit at its best the CANCO experiment. Indeed, being a constant-time experiment [35], the negative intensity of the correlation involving these residues are often a useful starting point for the sequential assignment for the different peptidic fragments.

In conclusion, extension to the third dimension and inclusion of a spin state selective approach to remove the large one bond C^{α}–C' splitting are key aspects to obtain a sufficient resolution to study complex systems by ^{13}C-direct detection NMR. All the experiments presented here include the IPAP method [22,36–39]. Among the alternative ways to obtain spin-state selection [37,40–42], the S^{3}E approach [40] may be actually better than the IPAP for higher molecular masses and higher magnetic fields, cases in which C' relaxation is faster. Indeed, despite less robust to variations in the C^{α}–C' coupling constant values than IPAP [41], it depends on $1/4J_{C^{\alpha}C'}$ rather than $1/2J_{C^{\alpha}C'}$, thus requiring half the time as the IPAP. Therefore, we implemented it in the pulse sequences where it contributes to reducing the overall duration of the experiment (CACO-S^{3}E [22], CBCACO-S^{3}E, and CCCO-S^{3}E). The details of the pulse sequences of CBCACO-S^{3}E and of CCCO-S^{3}E are reported in Appendix A.

3. Materials and methods

3.1. Sample preparation

The ^{13}C,^{15}N-labeled monomeric mutant F50E/G51E/E133Q of superoxide dismutase was expressed and purified as previously reported [28,33]. The protein concentration in the final NMR samples was about 1.5 mM. The copper was reduced under anaerobic conditions with sodium ascorbate. The buffer was 20 mM phosphate at pH 5.0 and 10% D_2O was added for the lock signal. All the spectra detailed below were recorded at 298 K.

3.2. NMR experiments

All the experiments reported were recorded at 14.1 T with a 600 Avance NMR spectrometer equipped with a triple-resonance cryoprobe optimized for ^{13}C sensitivity equipped with 3 cold preamplifiers (^{13}C, ^{1}H, and ^{2}H). The pulse lengths used were 11 μs for ^{13}C, 14.8 μs for ^{1}H and 40 μs for ^{15}N. Experiments were acquired placing the ^{1}H and ^{15}N carriers at 4.7 and 118 ppm respectively and ^{13}C pulses were given at 173, 55 and 39 ppm to excite or invert C', C^{α}, and $C^{\alpha/\beta}$ spins respectively unless otherwise specified. Composite pulse decoupling was applied during acquisition and during some of the elements of the pulse sequence with RF field strength of 2.9 and 1.0 kHz for ^{1}H (waltz-16) [43] and ^{15}N (garp-4) [44]. For ^{13}C the following pulses were used: 320 μs with Q5 (and time reversed Q5) shapes [45] for C^{α}, C^{ali} excitation, 256 μs Q3 shape and 1 ms Q3 shape [45] for C^{ali} and C^{α} inversion/refocusing respectively, 500 μs Chirp shape [46] for adiabatic inversion of C' and C^{α}. Experiments were acquired with relaxation delays between 1.4 and 1.5 s and acquisition times ranging from 141 to 159 ms. The spectral widths were between 18 and 24 ppm for C', 42 ppm for N, 48 ppm for C^{α}, and 75–80 ppm for C^{ali}.

The following 2D experiments were acquired: CACO-IPAP [22] (with 16 scans, 1024×256 data points), CBCACO-IPAP [22] (with 16 scans, 800×96 data points), CON-IPAP (with 32 scans, 800×256 data points), CANCO-IPAP (C^{α}–C' plane) (with 512 scans, 1024×192 data points), CCCO-IPAP with mixing times of 10, 15, and 22 ms (each spectrum with 16 scans, 1024×192 data points), CBCACO-S^{3}E (with 32 scans, 512×128 data points), CCCO-S^{3}E with mixing time of 12 ms (with 32 scans, 512×256 data points).

The following 3D experiments were acquired: CBCACO-IPAP [22] (16 scans, $800 \times 24 \times 96$ data points), CCCO-IPAP with mixing time of 22 ms (32 scans, $800 \times 32 \times 128$ data points), CBCACON-IPAP (32 scans, $800 \times 64 \times 128$ data points), CCCON-IPAP with mixing time of 22 ms (24 scans, $512 \times 32 \times 256$ data points), and CANCO-IPAP (512 scans, $1024 \times 16 \times 48$ data points).

For experiments that employ the IPAP approach in the acquisition dimension, linear combination of the in-phase and anti-phase components (that were stored separately), followed by a frequency shift of each of the two multiplet components to the center of the original doublet, was performed to suppress the C^{α}–C' coupling [22,47].

For experiments that employ the S^{3}E approach in the acquisition dimension, the sum of the first two FIDs (stored separately) gives one of the two multiplet components, while the difference, phase shifted by $\pi/2$ gives the

other multiplet component. Each of the two multiplet components is then shifted to the center of the original doublet to suppress the C^{α}–C' coupling [22,47].

The pulse sequences of CON-IPAP, CANCO-IPAP, CCCO-IPAP, CBCACON-IPAP, CCCON-IPAP, CBCACO-S^3E, and CCCO-S^3E are reported and described in detail in Appendix A.

Acknowledgments

Oskar Schett and Michael Fey (Bruker BioSpin AG) are acknowledged for the stimulating discussions. This work has been supported in part by the EC Contracts HPRI-CT-2001-50026, HPRN-CT-2000-00092, and QLG2-CT-2002-00988. All the NMR pulse sequences written for the Bruker Avance series spectrometers are available upon request.

Appendix A

The new pulse sequences to acquire the experiments described in the main text are described in detail hereafter. In particular we report the CCCO-IPAP, CBCACON-IPAP, CCCON-IPAP, the implementation of IPAP in the CON and CANCO experiments (CON-IPAP, CANCO-IPAP) as well as the implementation of the S^3E approach in the experiments in which this reduces the overall duration of the pulse scheme (CBCACO-S^3E, CCCO-S^3E). In all the figures reported hereafter, band selective ^{13}C pulses are denoted by shapes. For ^{13}C excitation and inversion/refocusing Q5 (or time reversed Q5) and Q3 shapes [45] were used with durations of 320 μs and 256 μs respectively unless for the pulse indicated in grey (Q3, 1 ms). The rectangular wide and narrow pulses correspond to π and π/2 flip angles. Pulse field gradients (PFG line) are also indicated by shapes. The ^{1}H and ^{15}N carriers are placed at 4.7 and 118 ppm, respectively. The change in the position of the ^{13}C carrier (39 ppm for C^{ali}, 55 ppm for C^{α} and 173 ppm for C') is indicated by vertical arrows. The RF power used for the ^{13}C FLOPSY16 spin-lock was 10 kHz (applied for durations ranging from 10 to 22 ms in the 2D versions and 22 ms in the 3D version). Decoupling of ^{1}H and ^{15}N was achieved with 2.9 kHz waltz-16 [43] and 1.0 kHz garp-4 [44] schemes respectively. The amount of decoupling is comparable to that necessary in conventional triple resonance experiments except for the additional ^{1}H decou-

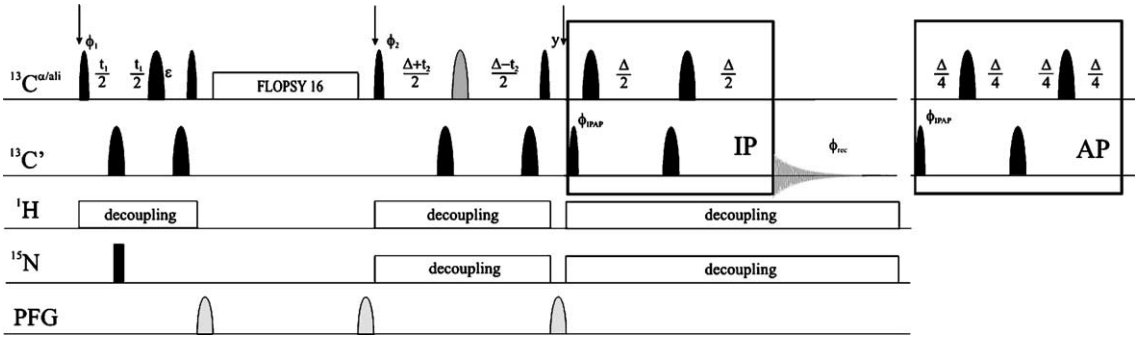

Fig. 6. CCCO-IPAP. The delays are: $\Delta = 9$ ms, $\varepsilon = t_1(0)$. The phase cycle is: $\phi_1 = x,-x$; $\phi_2 = 2x,2(-x)$; $\phi_{\mathrm{IPAP}}(\mathrm{IP}) = 4x,4(-x)$; $\phi_{\mathrm{IPAP}}(\mathrm{AP}) = 4(-y),4y$; $\phi_{\mathrm{rec}} = x,(-x),(-\mathrm{x}),x,(-x),x,x,(-x)$. Quadrature detection in the F_1 and F_2 dimensions is obtained by incrementing ϕ_1 and ϕ_2, respectively, in a States-TPPI manner. The strength of the gradients is 50%:60%:11%.

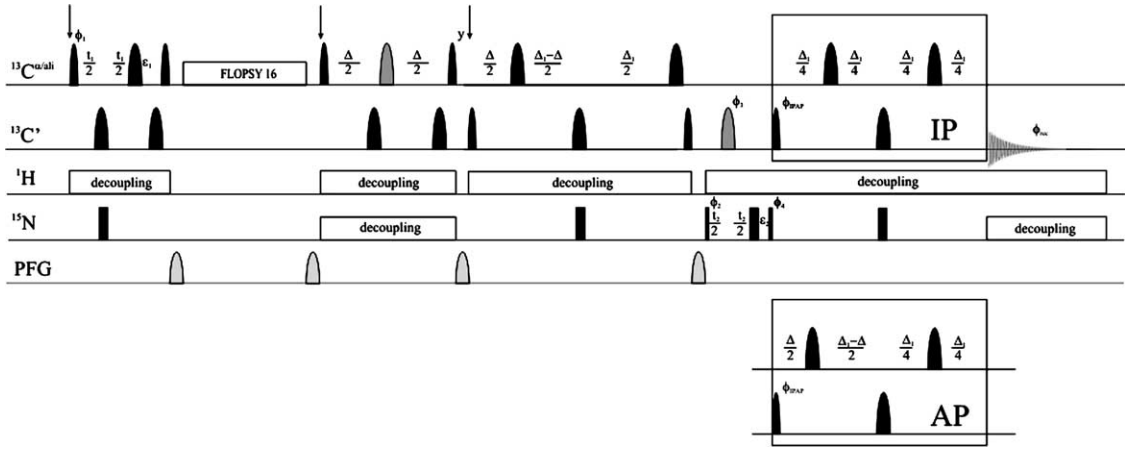

Fig. 7. CCCON-IPAP. The delays are: $\Delta = 9$ ms, $\Delta_1 = 25$ ms, $\varepsilon_1 = t_1(0)$, $\varepsilon_2 = t_2(0)$. The phase cycle is: $\phi_1 = x,-x$; $\phi_2 = 2x,2(-x)$; $\phi_3 = 4x,4(-x)$; $\phi_4 = 8x,8(-x)$; $\phi_{\mathrm{IPAP}}(\mathrm{IP}) = x$; $\phi_{\mathrm{IPAP}}(\mathrm{AP}) = -y$; $\phi_{\mathrm{rec}} = 2(x,(-x),(-x),x),2((-x),x,x,(-x))$. Quadrature detection in the F_1 and F_2 dimensions is obtained by incrementing ϕ_1 and ϕ_2, respectively, in a States-TPPI manner. The strength of the gradients is 50%:60%:19%:11%.

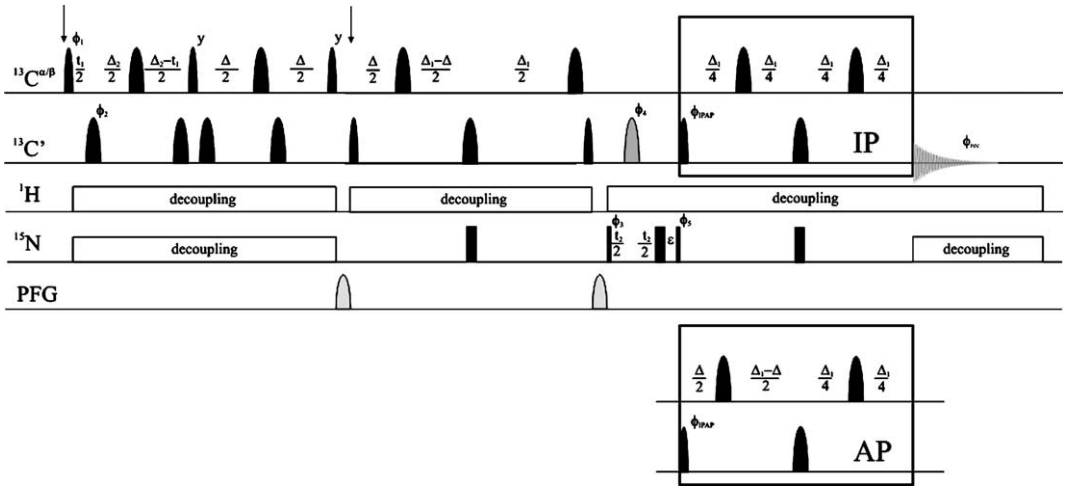

Fig. 8. CBCACON-IPAP. The delays are: $\Delta = 9$ ms, $\Delta_1 = 25$ ms, $\Delta_2 = 8$ ms $\varepsilon = t_2(0)$. The phase cycle is: $\phi_1 = x, -x$; $\phi_2 = -y$; $\phi_3 = 2x, 2(-x)$; $\phi_4 = 4x, 4(-x)$; $\phi_5 = 8x, 8(-x)$; $\phi_{\mathrm{IPAP}}(\mathrm{IP}) = x$; $\phi_{\mathrm{IPAP}}(\mathrm{AP}) = -y$; $\phi_{\mathrm{rec}} = 2(x,(-x),(-x),x), 2((-x),x,x,(-x))$. Quadrature detection in the F_1 and F_2 dimensions is obtained by incrementing ϕ_1 and ϕ_3, respectively, in a States-TPPI manner. The strength of the gradients is 30%:19%.

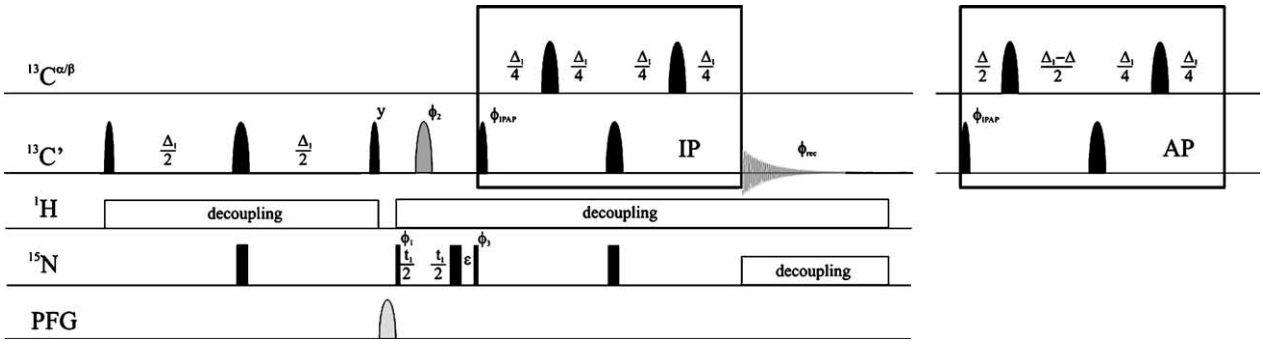

Fig. 9. CON-IPAP. The delays are: $\Delta = 9$ ms, $\Delta_1 = 25$ ms, $\varepsilon = t_1(0)$. The phase cycle is: $\phi_1 = x, -x$; $\phi_2 = 2x, 2(-x)$; $\phi_3 = 4x, 4(-x)$; $\phi_{\mathrm{IPAP}}(\mathrm{IP}) = x$; $\phi_{\mathrm{IPAP}}(\mathrm{AP}) = -y$; $\phi_{\mathrm{rec}} = x,(-x),x,(-x),(-x),x,(-x),x$. Quadrature detection in the F_1 dimension is obtained by incrementing ϕ_1 in a States-TPPI manner. The strength of the gradient is 30%.

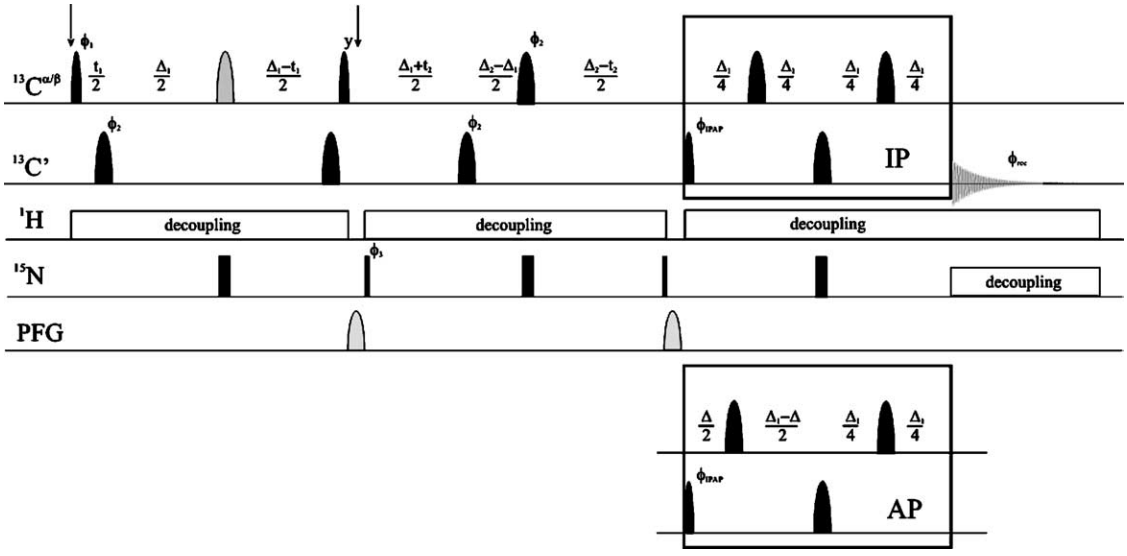

Fig. 10. CANCO-IPAP. The delays are: $\Delta = 9$ms, $\Delta_1 = 25$ ms, $\Delta_2 = 32$ ms. The phase cycle is: $\phi_1 = x, -x$; $\phi_2 = 8x, 8(-x)$; $\phi_3 = 2x, 2(-x)$; $\phi_{\mathrm{IPAP}}(\mathrm{IP}) = 4x, 4(-x)$; $\phi_{\mathrm{IPAP}}(\mathrm{AP}) = 4(-y), 4y$; $\phi_{\mathrm{rec}} = x,(-x),(-x)x,(-x),x,x,(-x)$. Quadrature detection in the F_1 and F_2 dimensions is obtained by incrementing ϕ_1 and ϕ_3, respectively, in a States-TPPI manner. The strength of the gradients is 30%:19%.

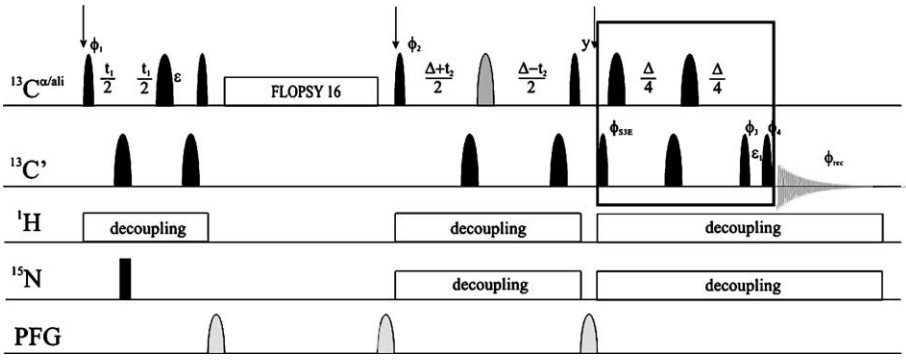

Fig. 11. CCCO-S^{3}E. The delays are: $\Delta = 9$ ms, $\varepsilon = t_1(0)$, $\varepsilon_1 = 4$ μs. The phase cycle is: $\phi_1 = x,-x$; $\phi_2 = 4x,4(-x)$, $\phi_3 = 2x,2(y)$, $\phi_4 = 2x,2(y)$, $\phi_{S^3E}(1) = 4(45°)$, $\phi_{S^3E}(2) = 2(45°),2(225°)$; $\phi_{rec} = x,(-x),(-x),x,(-x),x,x,(-x)$. Quadrature detection in the F_1 and F_2 dimensions is obtained by incrementing ϕ_1 and ϕ_2, respectively, in a States-TPPI manner. The strength of the gradients is 50%:60%:11%.

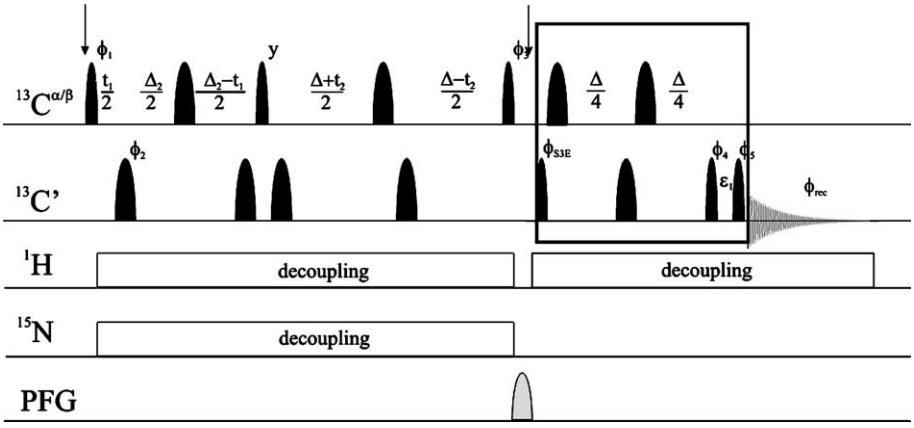

Fig. 12. CBCACO-S^{3}E. The delay Δ is 9 ms, $\Delta_2 = 8$ ms, $\varepsilon_1 = 4$ μs. The phase cycle is: $\phi_1 = x,-x$; $\phi_2 = 8x,8(-x)$; $\phi_3 = 2y,2(-y)$, $\phi_4 = 4x,4(y)$, $\phi_5 = 4x,4(y)$; $\phi_{S^3E}(1) = 4(45°),4(225°)$, $\phi_{S^3E}(2) = 8(45°)$; $\phi_{rec} = x,(-x),(-x),x,(-x),x,x,(-x)$. Quadrature detection in the F_1 and F_2 dimensions is obtained by incrementing ϕ_1 and ϕ_3 in a States-TPPI manner. The strength of the gradient is 30%.

pling during acquisition. For samples where this would be a concern, all decoupling, except during acquisition, can be replaced by π pulses. For experiments that employ the IPAP approach to suppress the C^{α}–C' coupling, the in-phase (IP) and anti-phase (AP) components are acquired and stored separately using the pulse schemes illustrated that differ only for the two panels indicated with IP and AP, respectively. For experiments that employ the S^{3}E approach to suppress the C^{α}–C' coupling, the two components that need to be acquired and stored separately differ by the phase φ_{S^3E} and by a π increment of phase φ_4 in the CCCO-S^{3}E experiment and φ_5 in the CBCACO-S^{3}E experiment. The phase cycle, the method used for quadrature detection, the durations of the delays shown in the pulse sequences and the strengths of the gradients, given as percentage of the maximum gradient strength of 53.5 G/cm (all gradients had a duration of 1 ms, a sine shape), are reported case-by-case (see Figs. 6–12).

References

[1] B.-H. Oh, W.M. Westler, P. Darba, J.L. Markley, Protein carbon-13 spin systems by a single two-dimensional nuclear magnetic resonance experiment, Science 240 (1988) 908–911.

[2] W.M. Westler, M. Kainosho, H. Nagao, M. Tomonaga, J.L. Markley, Two-dimensional NMR strategies for carbon-carbon correlations and sequence-specific assignments in carbon-13 labeled proteins, J. Am. Chem. Soc. 110 (1988) 4093–4095.

[3] W.M. Westler, B.J. Stockman, J.L. Markley, Correlation of carbon-13 and nitrogen-15 chemical shifts in selectively and uniformly labeled proteins by heteronuclear two-dimensional NMR spectroscopy, J. Am. Chem. Soc. 110 (1988) 6256–6258.

[4] K. Pervushin, R. Riek, G. Wider, K. Wüthrich, Transverse relaxation-optimized spectroscopy (TROSY) for NMR studies of aromatic spin systems in ^{13}C-labeled proteins, J. Am. Chem. Soc. 120 (1998) 6394–6400.

[5] V. Tugarinov, R. Muhandiram, A. Ayed, L.E. Kay, Four-dimensional NMR spectroscopy of a 723-residue protein: chemical shift assignments and secondary structure of malate synthase G, J. Am. Chem. Soc. 124 (2002) 10025–10035.

[6] V. Tugarinov, P.M. Hwang, J.E. Ollerenshaw, L.E. Kay, Cross-correlated relaxation enhanced ^{1}H-^{13}C NMR spectroscopy of methyl groups in very high molecular weight proteins and protein complexes, J. Am. Chem. Soc. 125 (2003) 10420–10428.

[7] E. Miclet, D.C. Williams Jr, G.M. Clore, D.L. Bryce, J. Boisbouvier, A. Bax, Relaxation-optimized NMR spectroscopy of methylene groups in proteins and nucleic acids, J. Am. Chem. Soc. 126 (2004) 10560–10570.

[8] R. Riek, J. Fiaux, E.B. Bertelsen, A.L. Horwich, K. Wuthrich, Solution NMR techniques for large molecular and supramolecular structures, J. Am. Chem. Soc. 124 (2002) 12144–12153.

[9] R. Riek, G. Wider, K. Pervushin, K. Wuthrich, Polarization transfer by cross-correlated relaxation in solution NMR with very large molecules, Proc. Natl. Acad. Sci. USA 96 (1999) 4918–4923.
[10] U. Kolczak, J. Salgado, G. Siegal, M. Saraste, G.W. Canters, Paramagnetic NMR studies of blue and purple copper proteins, Biospectroscopy 5 (1999) S19–S32.
[11] I. Bertini, Y.-M. Lee, C. Luchinat, M. Piccioli, L. Poggi, Locating the metal ion in calcium-binding proteins by using cerium(III) as a probe, ChemBioChem 2 (2001) 550–558.
[12] T.E. Machonkin, W.M. Westler, J.L. Markley, ^{13}C-^{13}C 2D NMR: a novel strategy for the study of paramagnetic proteins with slow electronic relaxation times, J. Am. Chem. Soc. 124 (2002) 3204–3205.
[13] M. Kostic, S.S. Pochapsky, T.C. Pochapsky, Rapid recycle ^{13}C, ^{15}N and ^{13}C,^{13}C heteronuclear and homonuclear multiple quantum coherence detection for resonance assignments in paramagnetic proteins: example of Ni^{2+}-containing acireductone dioxygenase, J. Am. Chem. Soc. 124 (2002) 9054–9055.
[14] F. Arnesano, L. Banci, I. Bertini, I.C. Felli, C. Luchinat, A.R. Thompsett, A strategy for the NMR characterization of type II copper(II) proteins: the case of the copper trafficking protein CopC from *Pseudomonas syringae*, J. Am. Chem. Soc. 125 (2003) 7200–7208.
[15] A. Eletsky, O. Moreira, H. Kovacs, K. Pervushin, A novel strategy for the assignment of side-chain resonances in completely deuterated large proteins using ^{13}C spectroscopy, J. Biomol. NMR 26 (2003) 167–179.
[16] I. Bertini, I.C. Felli, R. Kümmerle, D. Moskau, R. Pierattelli, ^{13}C-^{13}C NOESY: an attractive alternative to study large macromolecules, J. Am. Chem. Soc. 126 (2004) 464–465.
[17] N. Shimba, H. Kovacs, A.S. Stern, A.M. Nomura, I. Shimada, J.C. Hoch, C.S. Craik, V. Dötsch, Optimization of ^{13}C direct detection NMR methods, J. Biomol. NMR 30 (2005) 175–179.
[18] Z. Serber, C. Richter, D. Moskau, J.-M. Boehlen, T. Gerfin, D. Marek, M. Haeberli, L. Baselgia, F. Laukien, A.S. Stern, J.C. Hoch, V. Doetsch, New carbon-detected protein NMR experiments using cryoprobes, J. Am. Chem. Soc. 122 (2000) 3554–3555.
[19] Z. Serber, C. Richter, V. Dötsch, Carbon-detected NMR experiments to investigate structure and dynamics of biological macromolecules, ChemBioChem 2 (2001) 247–251.
[20] I. Bertini, L. Duma, I.C. Felli, M. Fey, C. Luchinat, R. Pierattelli, P.R. Vasos, A heteronuclear direct detection NMR experiment for protein backbone assignment, Angew. Chem. Int. Ed. 43 (2004) 2257–2259.
[21] W. Bermel, I. Bertini, I.C. Felli, R. Pierattelli, P.R. Vasos, A selective experiment for the sequential protein backbone assignment from 3D heteronuclear spectra, J. Magn. Reson. 172 (2005) 324–328.
[22] W. Bermel, I. Bertini, L. Duma, L. Emsley, I.C. Felli, R. Pierattelli, P.R. Vasos, Complete assignment of heteronuclear protein resonances by protonless NMR spectroscopy, Angew. Chem. Int. Ed. 44 (2005) 3089–3092.
[23] B. Vögeli, H. Kovacs, K. Pervushin, Measurements of side chain ^{13}C-^{13}C residual dipolar coupling in uniformly deuterated proteins, J. Am. Chem. Soc. 126 (2004) 2414–2420.
[24] I. Bertini, I.C. Felli, R. Kümmerle, C. Luchinat, R. Pierattelli, ^{13}C-^{13}C NOESY: a constructive use of ^{13}C-^{13}C spin-diffusion, J. Biomol. NMR 30 (2004) 245–251.
[25] I. Bertini, M. Piccioli, M.S. Viezzoli, C.Y. Chiu, G.T. Mullenbach, A spectroscopic characterization of a monomeric analog of copper-zinc superoxide dismutase, Eur. J. Biophys. 23 (1994) 167–176.
[26] L. Banci, I. Bertini, M.S. Viezzoli, E. Argese, E. Orsega, C.Y. Chiu, G.T. Mullenbach, Tuning the activity of Cu,Zn superoxide dismutase through site directed mutagenesis: a relatively active monomeric species, J. Biol. Inorg. Chem. 2 (1997) 295–301.
[27] L. Banci, M. Benedetto, I. Bertini, R. Del Conte, M. Piccioli, M.S. Viezzoli, Solution structure of reduced monomeric Q133M2 Copper, Zinc Superoxide Dismutase. Why is SOD a dimeric enzyme? Biochemistry 37 (1998) 11780–11791.
[28] L. Banci, M. Benedetto, I. Bertini, R. Del Conte, M. Piccioli, T. Richert, M.S. Viezzoli, Assignment of backbone NMR resonances and secondary structural elements of a reduced monomeric mutant of copper/zinc superoxide dismutase, Magn. Reson. Chem. 35 (1997) 845–853.
[29] D.S. Wishart, M.S. Watson, R.F. Boyko, B.D. Sykes, Automated 1H and 13C chemical shift prediction using the BioMagResBank, J. Biomol. NMR 10 (1997) 329–336.
[30] D.S. Wishart, B.D. Sykes, F.M. Richards, Relationship between nuclear magnetic resonance chemical shift and protein secondary structure, J. Mol. Biol. 222 (1991) 311–333.
[31] D.S. Wishart, B.D. Sykes, The ^{13}C chemical shift index: a simple method for the identification of protein secondary structure using ^{13}C chemical shift data, J. Biomol. NMR 4 (1994) 171–180.
[32] S. Grzesiek, A. Bax, Correlating backbone amide and side chain resonances in larger proteins by multiple relayed triple resonance NMR, J. Am. Chem. Soc. 114 (1992) 6291–6293.
[33] L. Banci, I. Bertini, F. Cramaro, R. Del Conte, A. Rosato, M.S. Viezzoli, Backbone dynamics of human Cu, Zn superoxide dismustase and of its monomeric F50/EG51E/E133Q mutant: the influence of dimerization on mobility and function, Biochemistry 39 (2000) 9108–9118.
[34] M. Sattler, J. Schleucher, C. Griesinger, Heteronuclear multidimensional NMR experiments for the structure determination of proteins in solution emplying pulsed field gradients, Progr. NMR Spectrosc. 34 (1999) 93–158.
[35] S. Grzesiek, A. Bax, Improved 3D Triple-Resonance NMR techniques applied to a 31 KDa protein, J. Magn. Reson. 96 (1992) 432–440.
[36] M. Ottiger, F. Delaglio, A. Bax, Measurement of J and dipolar couplings from simplified two-dimensional NMR spectra, J. Magn. Reson. 131 (1998) 373–378.
[37] P. Andersson, J. Weigelt, G. Otting, Spin-state selection filters for the measurement of heteronuclear one-bond coupling constants, J. Biomol. NMR 12 (1998) 435–441.
[38] L. Duma, S. Hediger, B. Brutscher, A. Bockmann, L. Emsley, Resolution enhancement in multidimensional solid-state NMR spectroscopy of proteins using spin-state selection, J. Am. Chem. Soc. 125 (2003) 11816–11817.
[39] L. Duma, S. Hediger, A. Lesage, L. Emsley, Spin-state selection in solid-state NMR, J. Magn. Reson. 164 (2003) 187–195.
[40] A. Meissner, J.O. Duus, O.W. Sørensen, Spin-state-selective excitation. Application for E.COSY-type measurement of J(HH) coupling constants, J. Magn. Reson. 128 (1997) 92–97.
[41] B. Brutscher, Accurate measurement of small spin-spin couplings in partially aligned molecules using a novel J-mismatch compensated spin-state-selection filter, J. Magn. Reson. 151 (2001) 332–338.
[42] M. Ottiger, F. Delaglio, J.L. Marquardt, N. Tjandra, A. Bax, Measurement of dipolar couplings for methylene and methyl sites in weakly oriented macromolecules and their use in structure determination, J. Magn. Reson. 134 (1998) 365–369.
[43] A.J. Shaka, J. Keeler, R. Freeman, Evaluation of a new broadband decoupling sequence: WALTZ-16, J. Magn. Reson. 53 (1983) 313–340.
[44] A.J. Shaka, P.B. Barker, R. Freeman, Computer-optimized decoupling scheme for wideband applications and low-level operation, J. Magn. Reson. 64 (1985) 547–552.
[45] L. Emsley, G. Bodenhausen, Gaussian pulse cascades: new analytical functions for rectangular selective inversion and in-phase excitation in NMR, Chem. Phys. Lett. 165 (1990) 469–476.
[46] J.-M. Boehlen, G. Bodenhausen, Experimental aspects of chirp NMR spectroscopy, J. Magn. Reson. Ser. A 102 (1993) 293–301.
[47] N.C. Nielsen, H. Thøgersen, O.W. Sørensen, Doubling the sensitivity of INADEQUATE for tracing out the carbon skeleton of molecules by NMR, J. Am. Chem. Soc. 117 (1995) 11365–11366.